

Projections: an old diagnostic tool revisited

David C. Henley

ABSTRACT

Many kinds of projections have been used to help analyze seismic data over the history of seismic exploration, probably the most familiar being the CMP stack. We explore here the topic of projections with an eye to adapting them for particular kinds of analysis. We present several kinds of projections applied to a 4D seismic experiment in central Alberta and discuss the possibilities for diagnostics in this setting.

While we draw no conclusions in this work, we review the topic of projections in order to stimulate thinking about new ways in which to summarize and analyze multi-dimensional data volumes.

INTRODUCTION

The notion of projections probably arose first in optics, where the concept of shining a beam of light through a transparency onto a screen perpendicular to the beam comes immediately to mind. We usually think of projecting the light beam normal to the transparency, or to the screen, but other projections can be obtained by rotating the normal of the plane of the transparency relative to the axis of the light source and screen. This results in projected images of the transparency which appear to be ‘thinner’, or to have a different aspect ratio than the original image. Furthermore, the screen need not be perpendicular to the light beam; and its orientation, too, affects the aspect ratio of the image. If more than one transparent mask is interposed between the light source and the projection screen, then clearly, the projected image on the screen is affected by several parameters, including:

- Angle of the screen relative to the light beam axis
- Rotational angle of each transparency
- Angle of the perpendicular axis of each transparency relative to the light beam axis
- The relative opacity of each transparency—even totally opaque objects can be projected

Altering any of these will change the resulting screen image. Not only can the shape and orientation of the image change, but its intensities or amplitudes can change as a result of changes in the registration of features on the two transparencies relative to the projection axis. As a crude way of visualizing this, think of making shadow puppets with your hands to amuse children, and remember how many possibilities there are for shadow images using just your two hands and their orientation to the light.

Another familiar example of a projection is an X-ray exposure. In the simplest case, a single projection through a body or body part conveys enough information for

appropriate medical intervention, while in other cases, several projections, at different angles, are required for complete diagnosis. By taking a large number of projections, whose beam angles span a full 360deg, a full 2D image perpendicular to the beam plane can be obtained—the well-known CT scan. In fact, CT technology is a prime example of one of the major applications of projections: determining properties and details of the interior of an area or volume by probing the target with a beam of energy originating outside its boundaries. One of two beam attributes is normally measured; beam intensity, or beam delay. Given the measurements from a large enough array of probing beams over a large enough selection of angles, the details of the interior of an area or volume can be reproduced exactly (Radon, 1917). Even a limited set of projections, however, can be used to localize anomalies without perfectly imaging them. When beam intensity is measured, the resulting image represents the density image (with respect to the type of beam energy) of the projected object; when beam delay (or time-of-flight) is measured, the image represents the velocity structure (relative to the type of energy) of the object.

Mathematically, for our purposes, a projection is a summation along a particular direction through a multi-dimensional array of values or samples. With seismic data, we use projections of both 2D data arrays (like trace gathers), 3D data arrays (like a collection of trace gathers from a 2D survey), or 4D data arrays (the trace gathers from a 3D seismic survey). In most cases, the purpose of a projection is to enhance or emphasize some feature in an array of data samples along a chosen projection direction characteristic of that feature. A characteristic of a projection is that it reduces the dimensionality of a set of data values by one, hence simplifying and summarizing the data, and hopefully enhancing some desired attribute. Below, we describe various operations on seismic data that are based on projections.

1D projections

Trace ensemble transforms

A trace ensemble is a group of seismic traces which typically share one common attribute, often a spatial coordinate or acquisition parameter. Examples are source gathers, receiver gathers, and common-midpoint (CMP) gathers. A projection can be created from such an ensemble by summing all samples in the gather along a particular direction through the gather. When the summation is parallel to time lines, the process is usually called stacking. We often collect the 1D traces that result from stacking a group of 2D ensembles (which constitutes a 2D projection) into a corresponding 2D array for display. We can, however, project a given trace ensemble along directions that are not parallel to sample times, in a process called ‘slant-stacking’; and if we collect all the traces generated by slant-stacking over a broad range of slant angles, we have the Radon Transform of the original trace ensemble, analogous to a CT scan of the trace ensemble. The original ensemble can be recovered (albeit with artifacts) using the inverse Radon Transform, which is just a series of ‘back-projections’ through the traces which constitute the Radon Transform. A number of variations of this procedure are possible, including projecting the data along curved paths instead of linear ones.

2D projections

Stacking trace ensembles

The simplest type of projection with which most of us are familiar is the summation of multiple traces from an ensemble of traces collected according to some common parameter. A CMP stacked section is just a collection of projections, each of which is the summation of traces selected by common midpoint (CMP). If we consider a set of source gathers acquired along a surface line (a standard 2D survey), the samples in that data set are identified by three coordinates; source position, receiver position, and recording time. Since the complete data set is a 3-dimensional array of data, we can form projections through it in any conceivable direction; and the purpose of this present study is to investigate which of these may have diagnostic value. In any case, projections which involve stacking a trace ensemble typically assume the projection is along constant time lines and parallel to some parameter dependent upon acquisition geometry, which can be used to collect traces into ensembles (see Figure 1a). Curved-path projections can be implemented simply by resampling and interpolating the original traces according to some rule (like NMO correction). Examples of projection-direction parameters are source location, receiver location, source-receiver sum (midpoint), source-receiver difference (offset distance), etc. Projections along these parametric directions are called common-source stacks, common-receiver stacks, common-midpoint (CMP) stacks and common-offset stacks, and each serves a particular imaging or diagnostic function:

- Common-source stacks display data characteristics that vary with source surface location, like source statics, source signature differences, source surface coupling characteristics (surface function), etc.
- Common-receiver stacks show data characteristics that vary with receiver surface location, like receiver statics and receiver coupling characteristics (surface function).
- Common-midpoint (CMP) stacks show data characteristics, for approximately flat-lying layers, that are common to the reflection points on all the layers—in other words, the reflection image.
- Common-offset stacks enhance data characteristics that depend on the raypath of seismic energy in the various layers.

It is interesting to notice that for these common projections, the ones which are based strictly on a single surface coordinate capture details pertaining to the surface, while the one based on the sum of two surface coordinates (CMP) captures subsurface reflections, and the one based on their difference (common-offset) enhances raypath variations. The concept schematic in Figure 1a illustrates the relationships of these common projections relative to a volume of 2D data consisting of ordered source gathers. Although the figure portrays the data volume as a cube, its actual shape depends upon the range of source and receiver points relative to the length of the line.

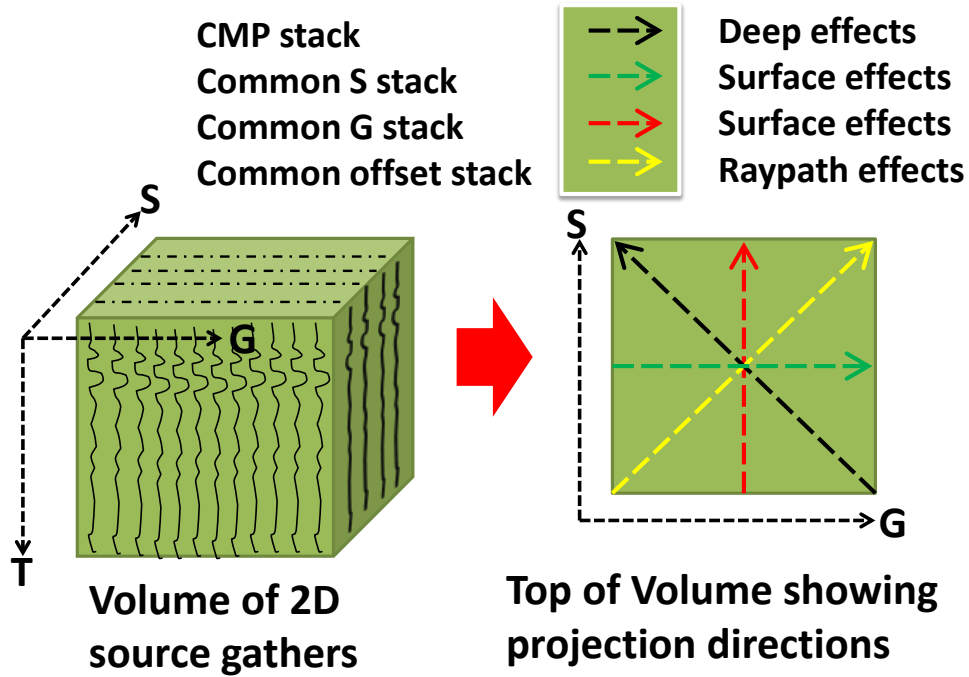


FIG. 1a. Schematic showing a data volume consisting of a set of source gathers (S) aligned by receiver station number (G). The top view shows the various commonly used projections (although the common-offset stack is used less than the individual common-offset gathers over which the summation is performed).

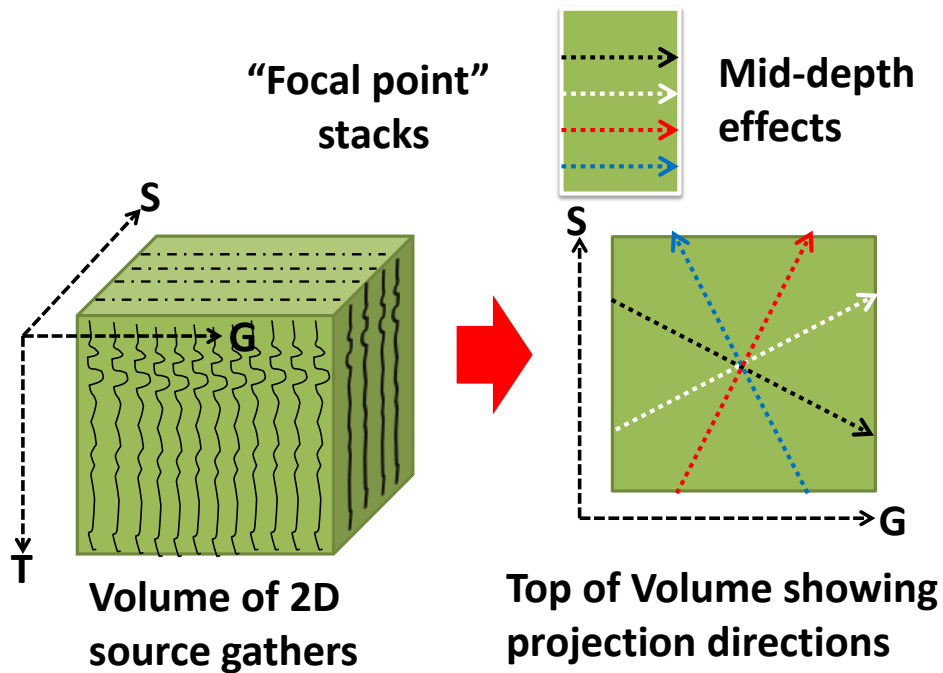


FIG. 1b., Schematic showing a 2D data volume projected along unconventional directions.

Other projections

Of course, there are other possibilities for defining projections through a set of 2D trace gathers, depending only upon our imagination and intuition. For example, consider projecting the 2D data volume in Figure 1a along directions other than those shown. Figure 1b shows some of these possibilities, to be discussed next.

Consider the schematic diagram in Figure 2, where the raypath geometry for a seismic reflection event is portrayed. By convention, the nominal reflection point of the raypath is identified by the midpoint of the raypath, referred to surface coordinates; hence the average of the surface locations of the source and receiver. It is only a small extension to create other linear combinations of source and receiver locations, which can be used to reference other parts of the raypath. Consider a general formula for a raypath surface coordinate:

$$(aS + bG)/(a + b) = FP_{ab}, \quad (1)$$

where S and G are surface location indices for source and receiver, respectively, a and b are positive integer weight parameters, and FP_{ab} is what we call a “Focal Point coordinate”, indexed by the weight parameters a and b . Clearly, when $b = a$, FP_{aa} is the CMP index associated with the midpoint of the reflecting raypath. In this formula, if either a or b is zero, the focal point becomes FP_{a0} , or FP_{0b} , and is equal to either the source location index or receiver location index, respectively. We can choose any positive integers we like for a and b , and in an obvious extension, use the corresponding FP_{ab} as a surface point location for a point on the raypath beneath the surface, as illustrated in Figure 3.

We know from our experience that projecting a 3D volume of 2D data along the FP_{aa} direction results in the CMP stack, in which anomalies along the reflector are highlighted. Also, we know that projecting along the FP_{a0} direction results in a common-source stack, which emphasizes source point anomalies (like statics); and projecting along the FP_{0b} direction produces the common-receiver stack, which enhances receiver point anomalies. It is a logical extension, then, to assume that projecting data along a general FP_{ab} direction will highlight anomalies associated with the point on a raypath directly beneath the FP_{ab} surface location. Because such anomalies are not directly associated with a location on a reflector or the surface, we term them “focal depth” anomalies, harking back to an early practice in statics correction methods where residual time anomalies which could not be associated with surface-consistent statics corrections were distributed to seismic traces along a “focal plane” which was typically chosen to be just beneath the surface layer.

To flesh out this idea somewhat, projections along an arbitrary FP_{ab} direction can be produced merely by creating an appropriate FP_{ab} trace header for each trace in a data set, using equation (1) with a particular choice of a and b . Sorting the traces, using the new trace header as the primary sort key then arranges the traces for the projection (stacking all traces with the value of FP_{ab} in common). If we anticipate projecting our data set along a number of different focal depth directions, all the new trace headers can easily be created at once, to facilitate subsequent trace sorting. In particular, it makes sense to create complementary pairs of focal depth headers, FP_{ab} and FP_{ba} . If the particular 2D

data set was acquired using surface sources, then we expect source and receiver statics to be similar at common locations, and we would expect complementary focal depth anomalies to be similar at the same surface location, as well, due to reciprocity. Figure 4 shows two such raypaths intersecting at a common focal depth. In this case,

$$(aS_1 + bG_1) = (bS_2 + aG_2), \quad (2)$$

where S_1 and G_1 are the indices of the source and receiver for one raypath, and S_2 and G_2 are the indices of the source and receiver for the other raypath. Of course, these aren't the only two raypaths passing through this focal depth point, since many choices of S and G will yield the same FP_{ab} in equation (1) for a single choice of a and b . Hence, summing all the traces from a 2D survey with a common value of FP_{ab} , for a particular choice of a and b constitutes a 'focal depth projection'. One use of such projections is to correct all the 'anomalies' seen on each projection—a simple extension of statics correction. This suggests a potential method for applying 'nonstationary' static corrections, which by definition vary with depth. We expand this idea in the next section.

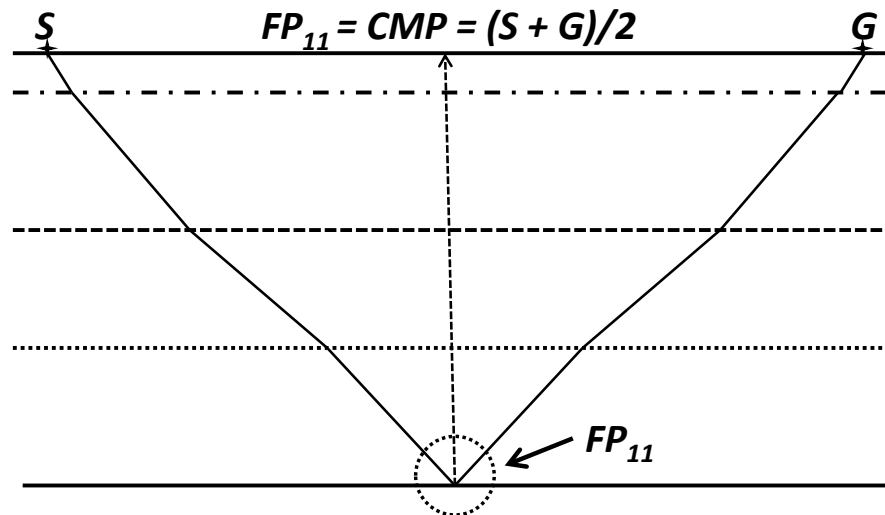


FIG. 2. Schematic showing typical raypath geometry for a conventional seismic trace for a single reflecting horizon. Using our "focal point" notation, the projected surface location of the reflection point (the raypath midpoint, for flat layers) is the simple average of the source and receiver surface locations. Many traces can share the same CMP, or FP_{11} , as long as the respective sums of their S and G locations are identical. "Projecting seismic data along FP_{11} " amounts to simply summing all traces with the same FP_{11} , or CMP.

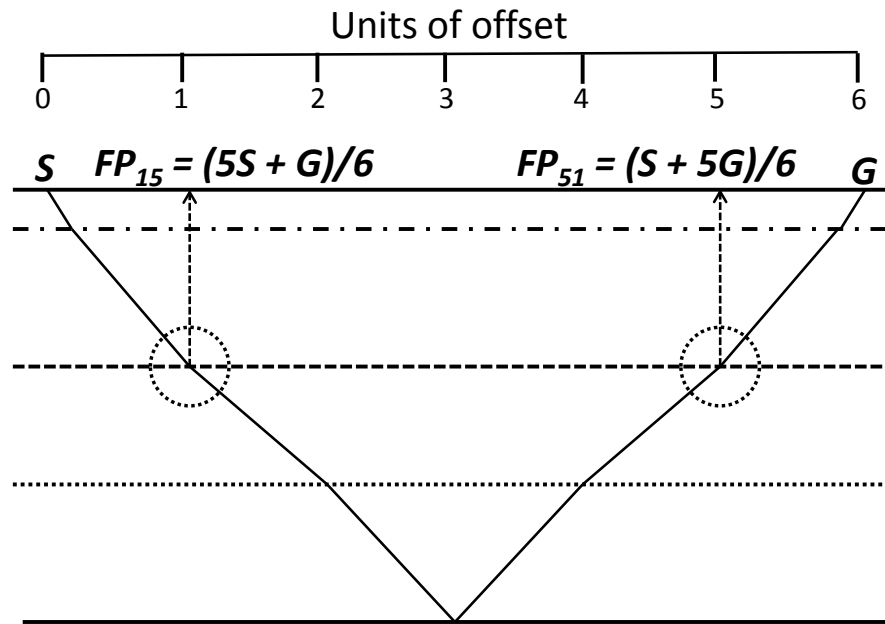


FIG. 3. Schematic showing other possible focal points along the raypath for a single reflecting horizon seen by a conventional seismic trace. The projected surface locations of these focal points are a simple weighted arithmetic mean of the S and G locations, where the weights are the reciprocal distances from the focal point surface location to S and G, respectively.

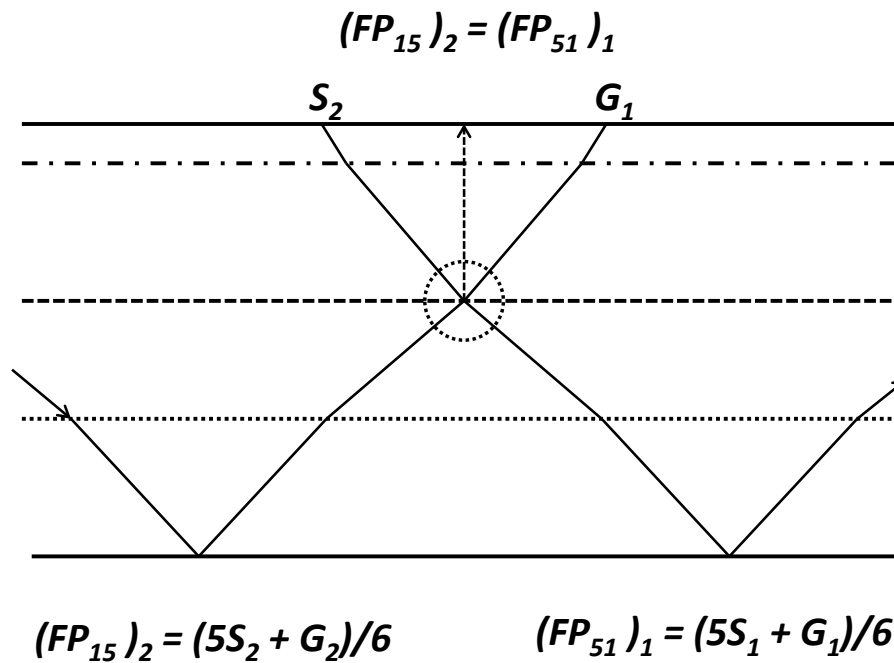


FIG. 4. Schematic showing raypaths from the same reflecting horizon which share a focal point. Reciprocity is assumed in this case. Obviously, many traces will share the same FP_{15} , or FP_{51} as long as the S_1 and G_1 , or S_2 and G_2 coordinates of the traces satisfy one of the formulas above. Projecting seismic traces along FP_{15} and/or FP_{51} hence amounts to summing all traces with the same value for these focal point locations.

A possible path to nonstationary statics correction

We outline here an idea for nonstationary statics correction by using projections of 2D data sets:

- Apply NMO corrections to all traces with the best available NMO function.
- Create new trace headers FP_{ab} using equation (1) for several choices of a and b , ensuring full complementarity to take advantage of reciprocity.
- Starting with the surface projections along directions FP_{0b} and FP_{a0} , find the trace-to-trace shifts in the projections and store the shifts in new individual trace headers on the raw traces. These correspond to conventional S and G static corrections.
- Apply the trace header shifts to the raw traces, then project traces along FP_{1b} and FP_{a1} , find the trace-to-trace shifts in these projections and store the shifts in new trace headers on the raw traces. These, we will call ‘focal depth’ corrections.
- Repeat for all complementary pairs of a and b up to $a = b$.

In this proposed procedure, the first step would amount to applying surface-consistent statics, and the last step would amount to applying trim statics to flatten the reflecting horizons. Each intermediate step, using focal plane projections would attempt to correct for any departures from stationarity by detecting and applying trace shifts attributable to anomalous pockets of earth material along the intermediate focal planes.

Projections in other domains

There is no reason, of course, that projections should be limited to the XT domain. One domain, in fact, which we utilize later in our demonstration of projections on real data is the Radial Trace (RT) domain. In particular, we will demonstrate the common-raypath stack and show its relation to the common-offset stack in the XT domain.

DEMONSTRATING PROJECTIONS

Violet Grove 4D experiment

We chose to illustrate the use of projections of various kinds using two sets of field seismic data that constitute a time-lapse, or 4D experiment, in which the goal is to detect differences in the seismic response of a particular rock layer over a period of time caused by injecting a fluid into the rock. The Violet Grove experiment, conducted over the years 2005-2007, attempted to monitor the injection of CO₂ into a porous formation conceived as a potential site for sequestration operations (Lawton et al, 2005; Coueslan et al, 2005, Chen and Lawton, 2005; Lu et al, 2005). From this experiment, which involved baseline and monitor surveys using 2D, 3D, and VSP surveys, we chose to examine only the 2D vertical component surveys, at least partly because the effect was expected to be only marginally detectable on these data. A number of studies have already examined these data (Alshuhail and Lawton, 2007), and several have used advanced techniques to

enhance detectability (Almutlaq and Margrave, 2012). In this study, however, our purpose is simply to investigate the use of various projections in conjunction with elementary processing to attempt to make the time-lapse anomaly more visible.

Comparing CMP projections

The 2D seismic surveys performed over the Violet Grove injection well were designed to be as nearly alike as possible, occupying the same source and receiver stations, and duplicating other conditions as closely as possible. The formation chosen for the CO₂ injection test was the Cardium, a (unfortunately) low-contrast horizon visible on the stacked CMP sections at a travel time just slightly greater than 1000ms. The presence of many high-contrast reflection events below the Cardium, as well as one strong event (Ardley) above the Cardium at 400ms means that time-lapse differences in the Cardium are difficult to observe, because of the low contrast. The shallow Ardley event can be relatively reduced in contrast by appropriate processing, since it is spaced well above the Cardium, but deeper strong events immediately beneath the Cardium are more of a challenge. To illustrate the difficulty, Figure 5 shows the CMP stack of the 2005 2D survey, and Figure 6 shows the corresponding 2007 survey; both have the zone of the expected anomaly outlined. As can be seen in the figures, the Cardium event is quite faint on both images, ironically, appearing faintest where the time-lapse anomaly is expected. The processing which yielded these two projections was as similar as possible so that the two could be compared by subtraction, in hopes that the time-lapse anomaly would be larger in amplitude than any residuals on other events.

The results of simple subtraction, shown in Figure 7, are disappointing and lead us to believe that there are factors affecting the amplitudes of the traces which differ between the two surveys. In any case, in Figure 7, the image differences manifested by the residual near-surface noise and by the reflections deeper than 1200ms are much larger than any potential anomaly in the target zone. In an attempt to better resolve image differences related only to the time-lapse, we applied a subtraction technique called 'least-squares subtraction' in which the slowly varying trace amplitude is matched exactly between traces being compared, leaving only the rapidly varying amplitude differences to highlight anomalies. Figure 8 shows the least-squares difference between the CMP images of the 2005 and 2007 surveys. While the surface noise residual is still prominent (probably due to differences in surface coupling between the two surveys), the deep reflections no longer dominate this difference image, and the amplitude differences that occur within the anomalous region are more prominent. Whether this is a legitimate time-lapse anomaly is still questionable, due to the relatively high level of mismatch still shown in this difference image. Although the difference of CMP images that directly portray the seismic response of a target layer are our best hope for detecting anomalies due to time-dependent changes in a subsurface target zone, we next examine other possible projections for their diagnostic value.

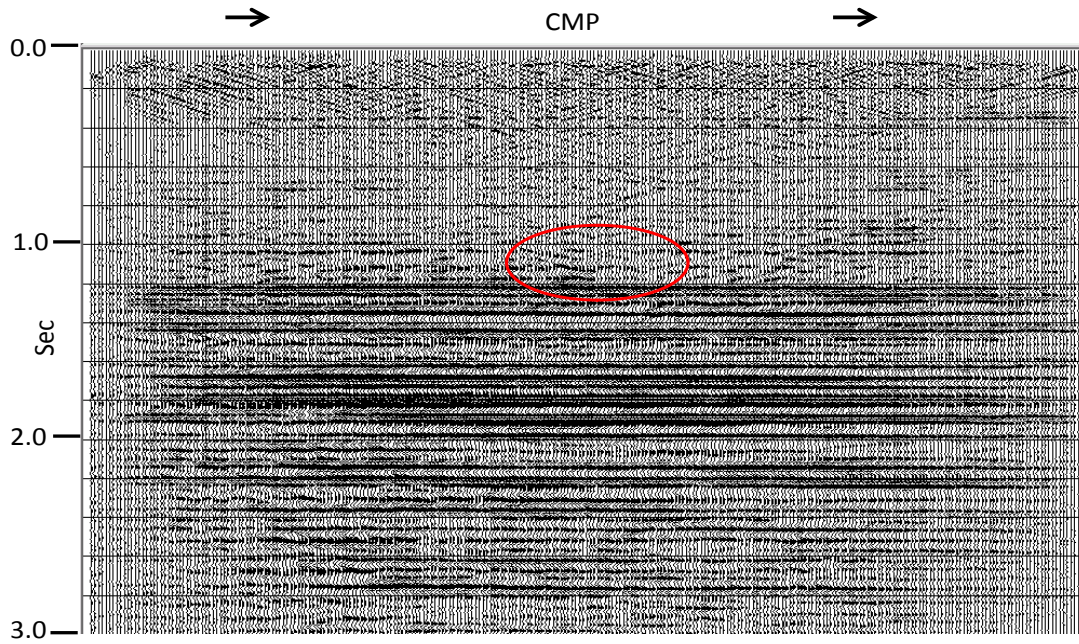


FIG. 5. The CMP stack (FP₁₁ projection) for the 2D seismic survey performed at Violet Grove in 2005, prior to beginning trial injection of CO₂. This is the 'baseline' survey for the 4D experiment.

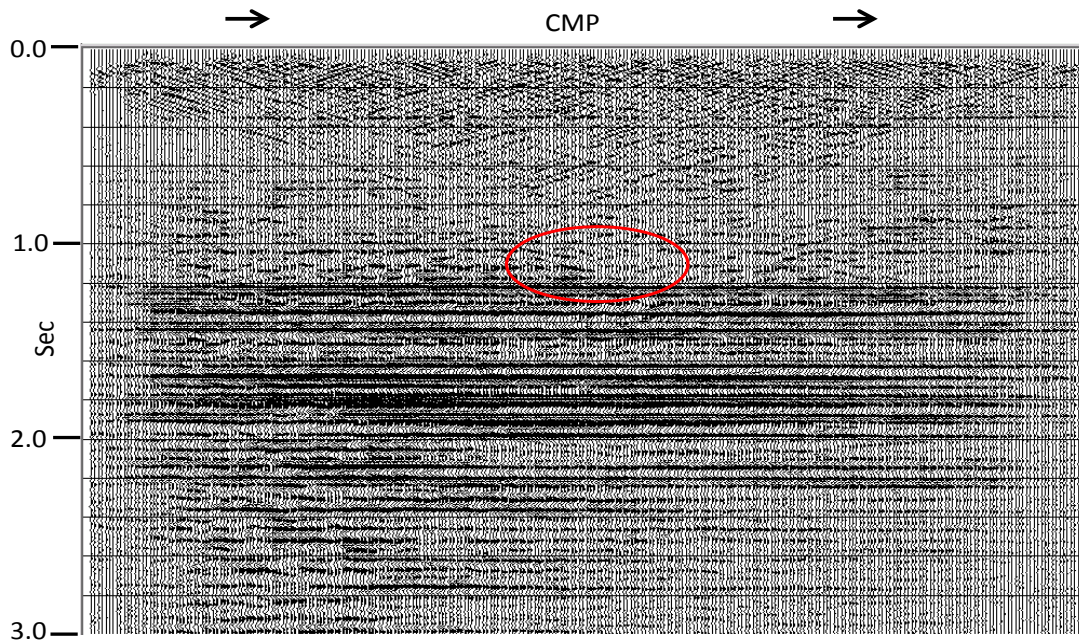


FIG. 6. The CMP stack (FP₁₁ projection) for the 2D seismic survey performed at Violet Grove in 2007, after commencement of the CO₂ injection. This is the time-lapse survey for the 4D experiment.

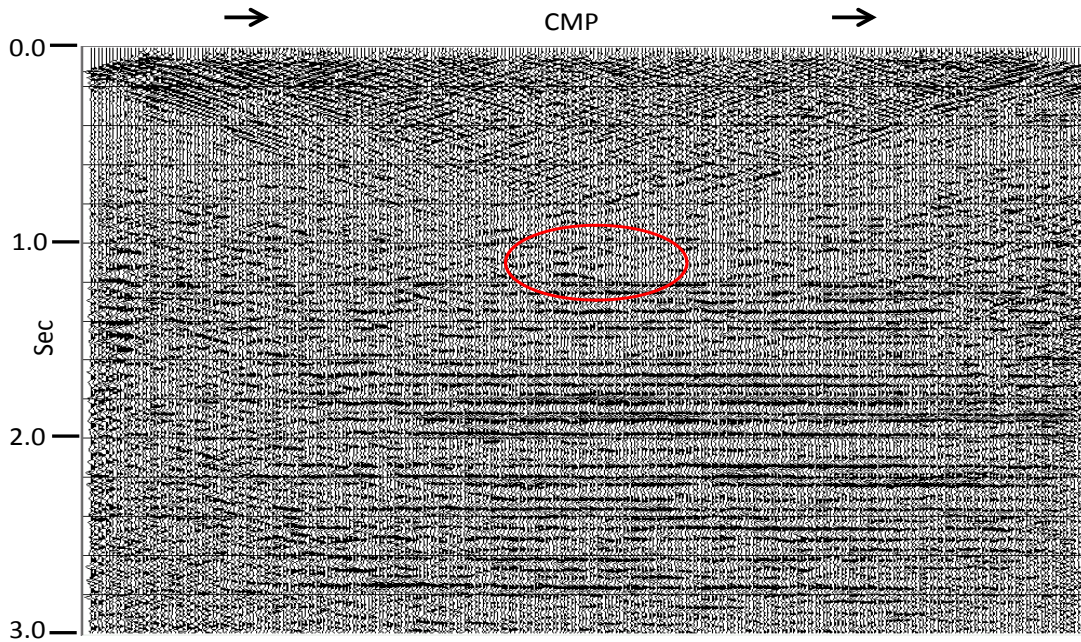


FIG. 7. The arithmetic difference between the projections (stacks) in Figures 5 and 6. The amplitude differences for the deeper reflectors are much larger than any apparent differences at the level of the injection zone (Cardium horizon at just below 1.0sec).

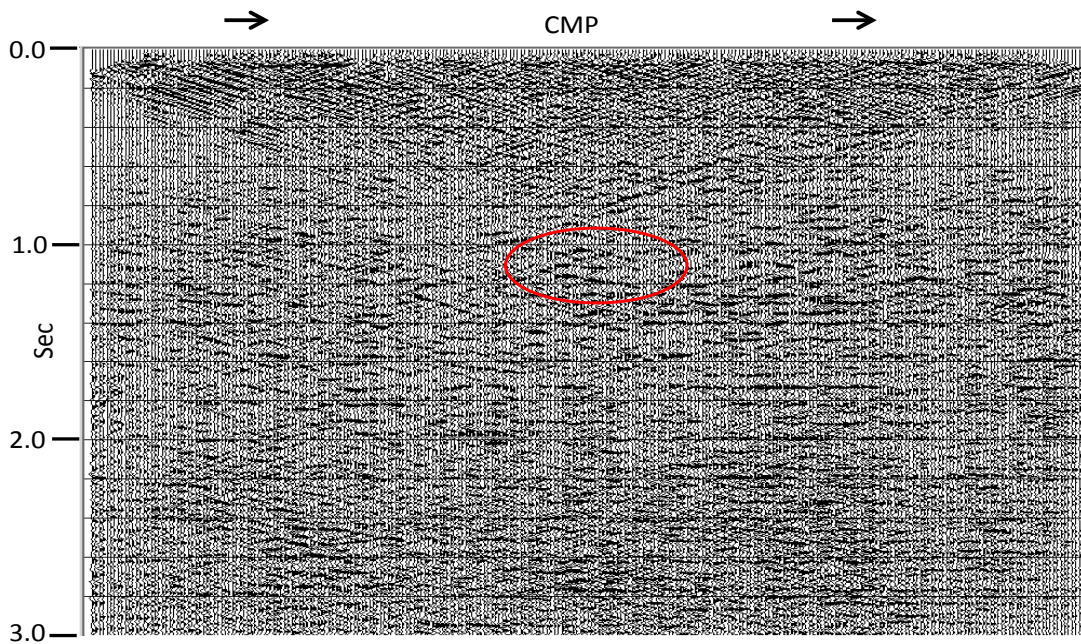


FIG. 8. The least squares difference between the projections in Figures 5 and 6. The residual amplitude differences for the deeper reflectors are much smaller than in Figure 7—but no unambiguous Cardium anomaly appears.

Comparing surface projections

Two possible projections to test are the common-source stack and the common-receiver stack, although we expect these projections to be more affected by differences in acquisition geometry and surface conditions than by our time-lapse anomaly at depth. Nevertheless, Figure 9 is the common-source stack of the 2005 survey, while Figure 10 is the comparable stack for 2007. Judging from Figure 9, the source statics for the 2005 survey were well-corrected, since there is no visible jitter on any of the reflecting horizons. Figure 10, on the other hand, shows that the source statics for the 2007 survey are less satisfactory, with visible static jitter appearing at all reflection levels. It is no surprise, then, that the image difference in Figure 11 shows significant mismatch. The least-squares difference in Figure 12, however, while it reduces the systematic mismatch due to slowly varying trace amplitude mismatch (as in the CMP stack comparison), still shows significant mismatch at particular traces where the statics mismatch is presumably greatest.

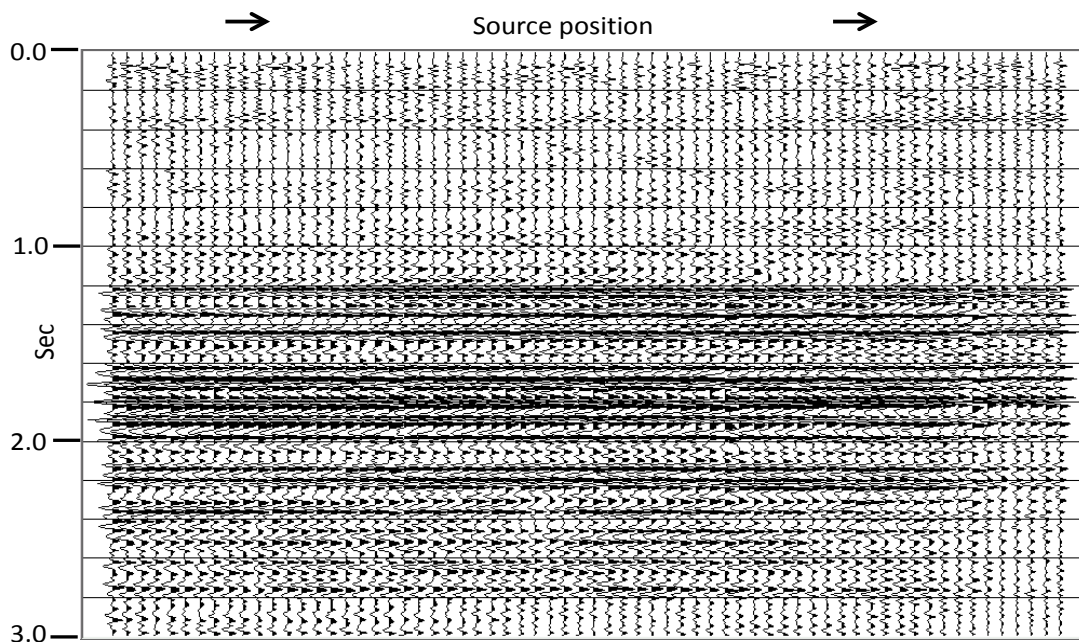


FIG. 9. The common-source stack (FP₀₁ projection) for the 2D Violet Grove 'baseline' survey performed in 2005. The absence of trace-to-trace static "jitter" indicates that the statics corrections for these data were good.

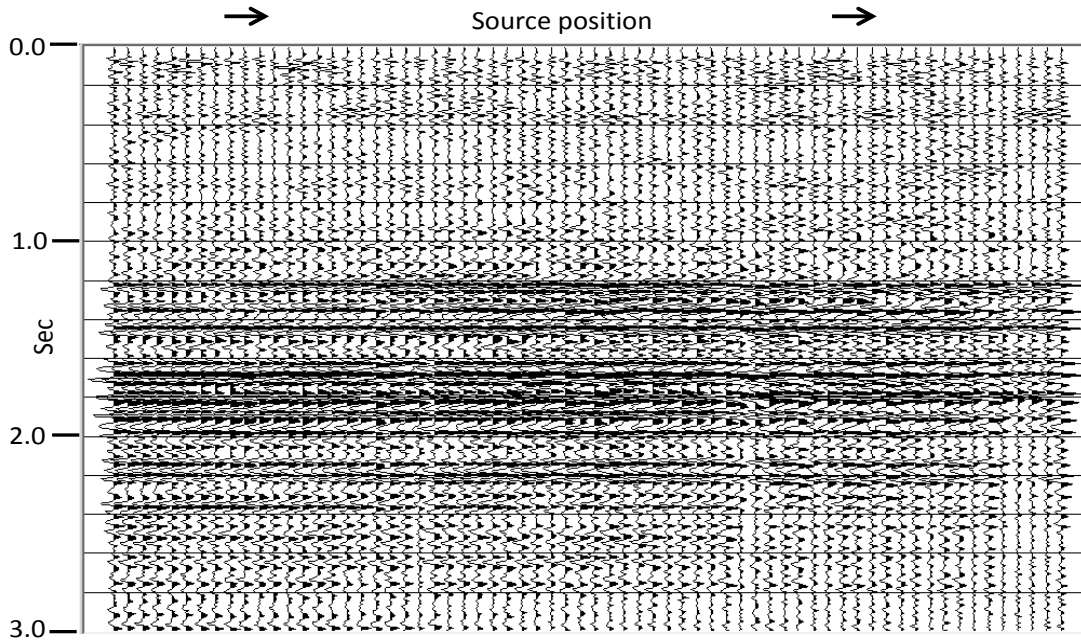


FIG. 10. The common-source stack (FP₀₁ projection) for the 2D Violet Grove 'time-lapse' survey performed in 2007. Comparison with Figure 9 shows a less satisfactory statics solution, as well as random lateral amplitude variations.

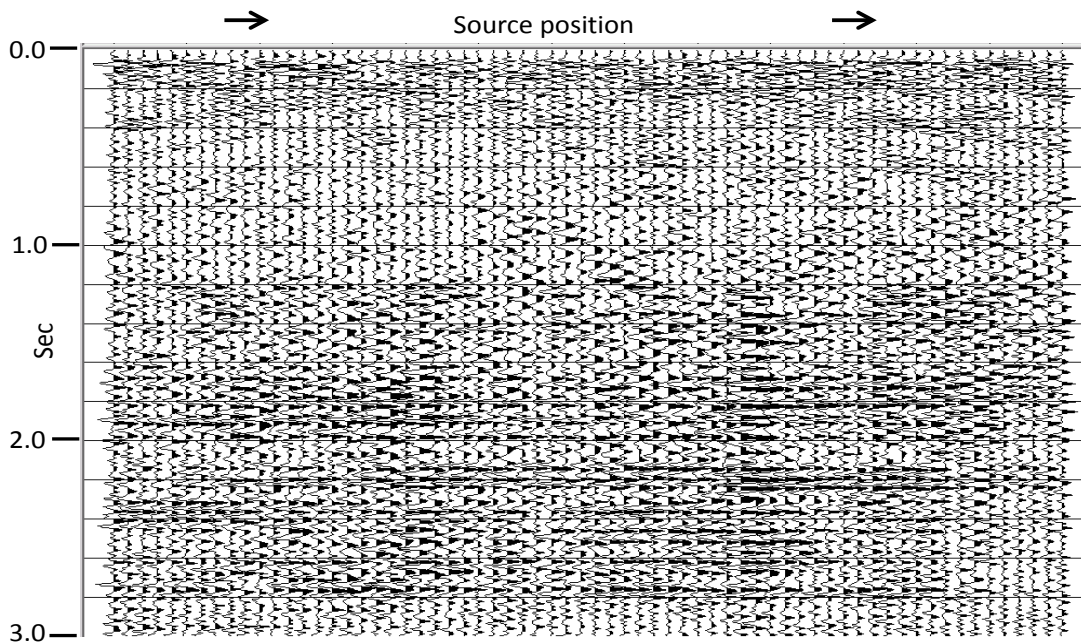


FIG. 11. Arithmetic difference between Figures 9 and 10. Residuals from statics differences and amplitude variations dominate the image. No particular anomaly visible.

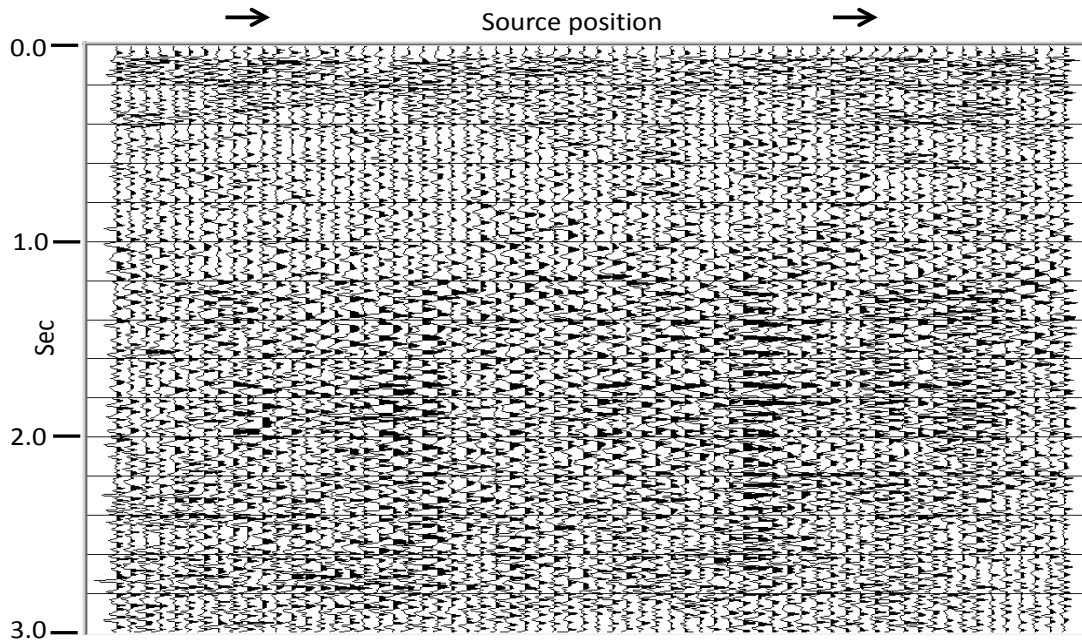


FIG. 12. Least-squares difference between Figures 9 and 10. Residuals from statics differences are still visible. No particular anomaly visible.

Likewise, Figures 13, 14, 15, and 16 show the common receiver stacks for 2005 and 2007, respectively, as well as their image differences and least-squares image differences. In this case, we can see some statics jitter for the common-receiver stack of the 2005 data (Figure 13), but significantly increased jitter for the 2007 common-receiver stack (Figure 14). In addition, we see different patterns of amplitudes on the two projections, as well as a higher level of residual coherent and random noise on the 2007 data. The overall systematic trace amplitude differences between the two vintages of data dominate Figure 15, while the statics mismatch causes much of the mismatch highlighted in Figure 16. As expected, the common-source and common-receiver projections serve best to diagnose image differences that are due to near-surface phenomena like statics differences and surface coupling (both presumably related primarily to seasonal differences at the surface during acquisition).

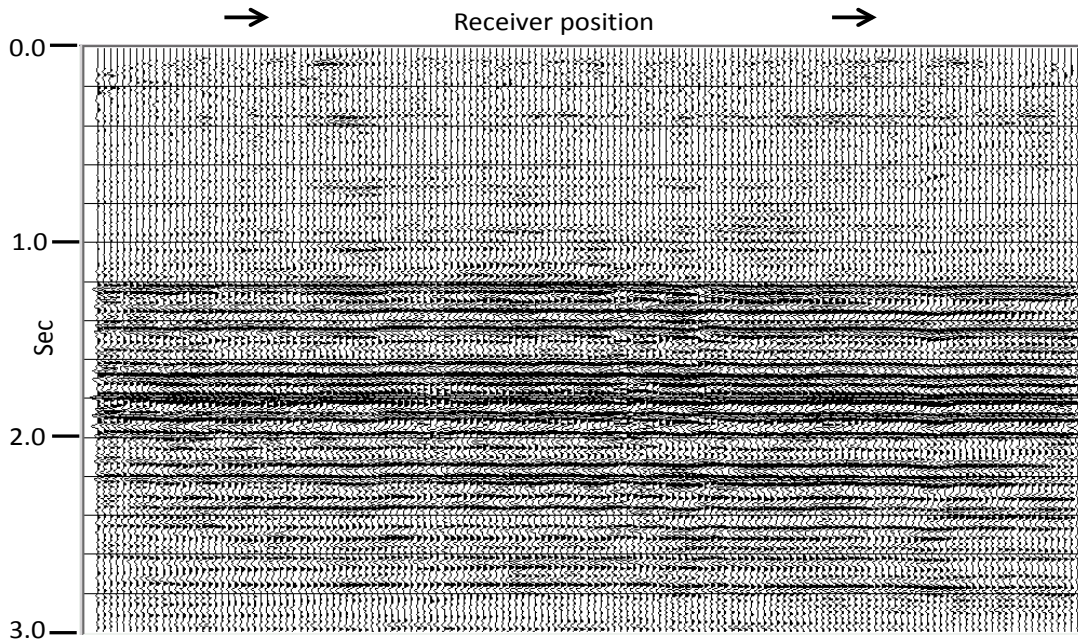


FIG. 13. Common-receiver stack (FP₁₀ projection) for the 2D Violet Grove 'baseline' survey performed in 2005. Some small static "jitter" is visible.

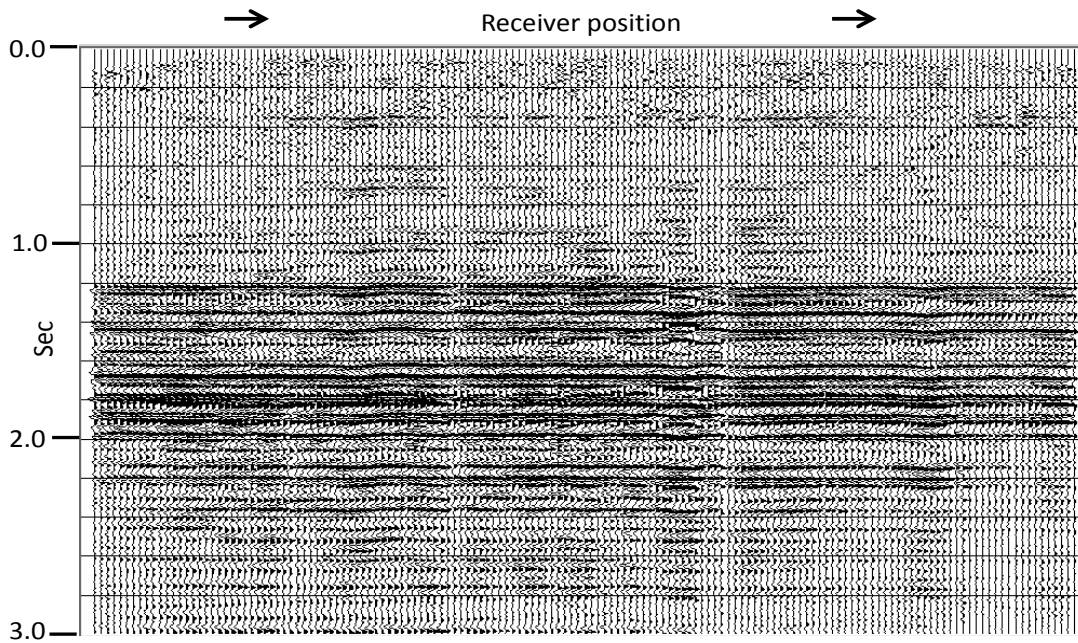


FIG. 14. Common-receiver stack (FP₁₀ projection) for the 2D Violet Grove 'time-lapse' survey performed in 2007. More static jitter, lateral amplitude variations, and greater random noise when compared with Figure 13.

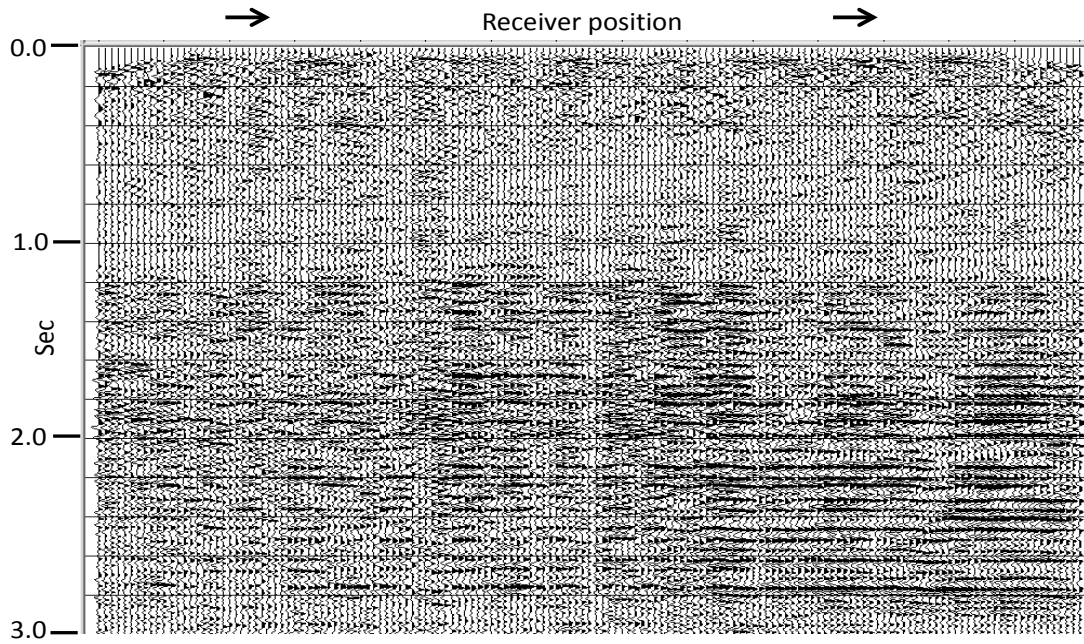


FIG. 15. Arithmetic difference between Figures 13 and 14. Residuals from amplitude variations and statics differences dominate. No apparent anomaly in the Cardium,

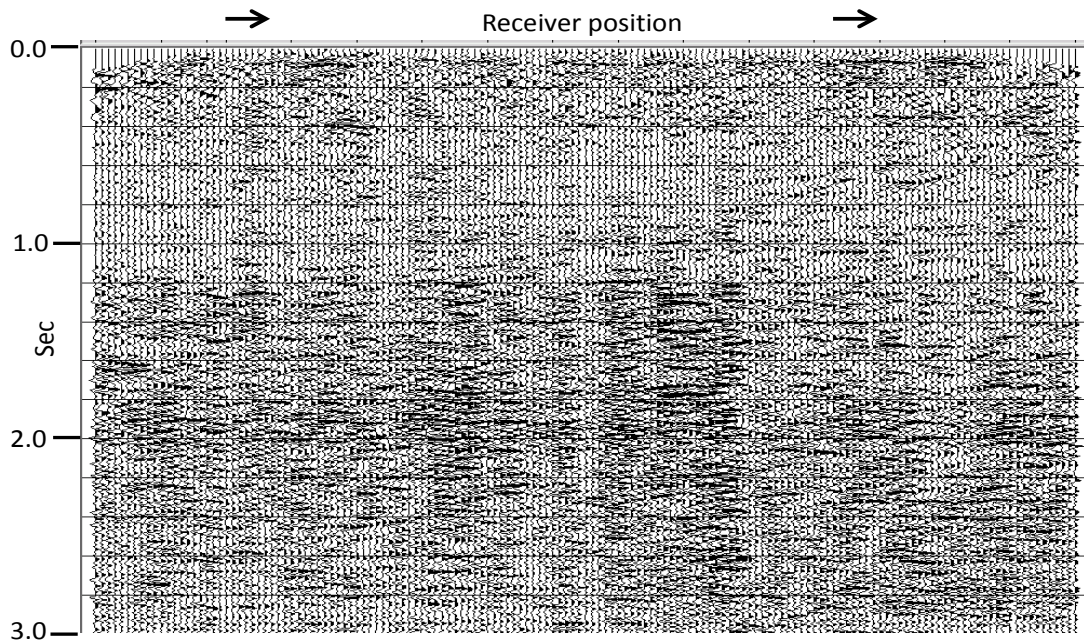


FIG. 16. Least-squares difference between Figures 13 and 14. Amplitude residuals are reduced, but static anomalies persist. No visible Cardium anomaly.

Other projections

Most of us will be familiar with common-offset gathers, since they can be used to analyze AVO effects and are sometimes the preferred feed for pre-stack migration algorithms. The concept of a common-offset stack is less familiar. Essentially, summing the traces in each common-offset gather to perform the common-offset projection destroys surface location information in order to enhance the offset dependence of each reflection event. Hence, when viewing a common-offset stack, we must remember that lateral position on the panel at any reflecting horizon relates only to source-receiver separation, not to lateral position along the horizon. What can be observed for any reflector is the variation of reflection amplitude with offset, which is directly correlated to the reflectivity as a function of raypath angle. Now, we can describe the common-offset projection using notation similar to that introduced earlier:

$$(aS - bG) = CD_{ab}, \quad (3)$$

Where S and G are the surface location indices for source and receiver, respectively, and CD_{ab} is the weighted arithmetic difference. Since each CD_{ab} does not correspond to an actual physical location like the various FP_{ij} (focal points), we use CD (coordinate difference) to designate the variable name, and the indices to designate the weights of the surface coordinates subtracted. At this point, the equally weighted difference CD_{11} is the only one that makes intuitive sense, but other possibilities obviously exist. Since S and G are located relative to a common origin for the survey, their difference destroys this absolute location information. Thus, projections along CD_{11} lose their location relative to surface coordinates for the survey, but acquire raypath discrimination in exchange.

For example, on the common-offset stack for the 2005 survey, shown in Figure 17, we see a typical reflection amplitude variation for the Ardley formation at 400ms, where the strongest amplitudes are at the smallest offsets and die away with increasing offset. This formation is such a good reflector that it tends to ‘shade’ the reflections beneath, whose amplitudes are somewhat diminished near zero offset. On this display, the Cardium (1000ms) is easily visible, but exhibits diminished amplitudes at smaller offsets. The comparable display for the 2007 survey is shown in Figure 18. Here, as well, we see apparent ‘shading’ by the Ardley; but the Cardium is visible, with similar amplitudes to those in Figure 17.

Now, since the time-lapse anomaly we seek is actually a localized change in the rock properties of the Cardium reflection, why would we expect to see the anomaly in a common-offset stack, where location information has been lost? The answer is that we might well expect to see rock property differences more prominently as a function of angle (or offset) than as a function of lateral position. Hence, when we subtract the images in Figures 17 and 18 to give Figure 19, we’re looking for significant amplitude “blooms” covering some range of offsets (both positive and negative). We do, in fact, observe such a pattern on Figure 19, along with a significant amplitude enhancement of the upper surface of the Cardium centred on zero offset. On the other hand, the systematic slowly-varying trace amplitude differences of the deep reflectors are also of significant amplitude. These artifacts are greatly reduced by the least squares difference in Figure 20, but so are the amplitude “blooms” at the lower boundary of the Cardium. The anomaly at the upper surface of the Cardium remains, however, and is about the

same amplitude as on Figure 19, lending some credibility to it as an actual detection of the desired time-lapse anomaly.

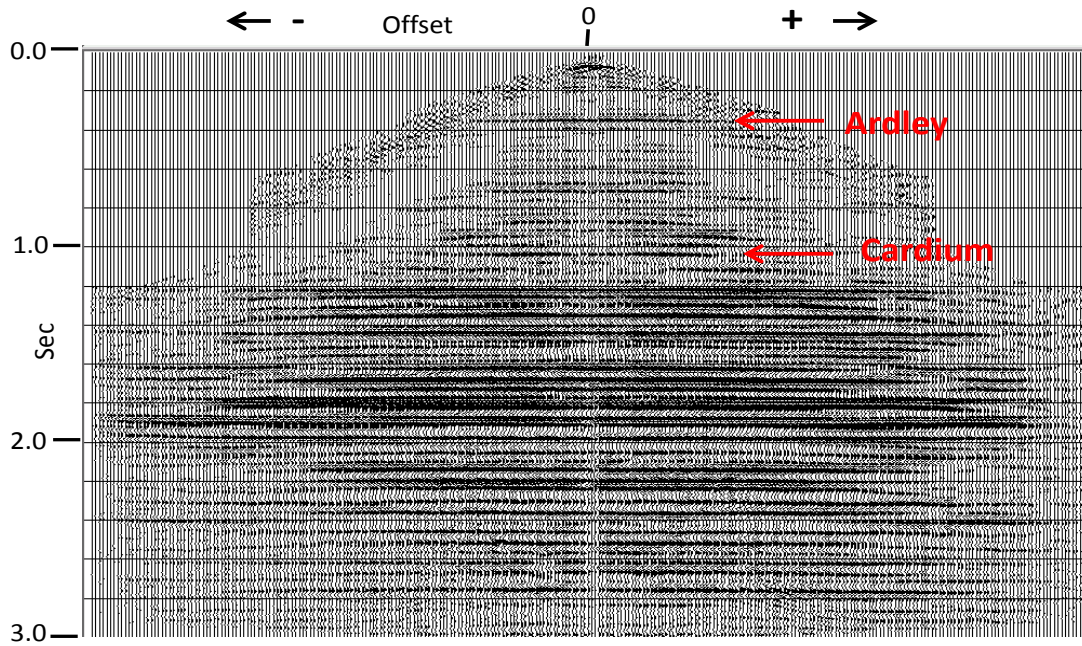


FIG. 17. Common-offset stack (CD₁₁ projection) for the 2D Violet Grove 'baseline' survey in 2005. Shading of deeper reflections by the strong Ardley reflection at 400ms is visible.

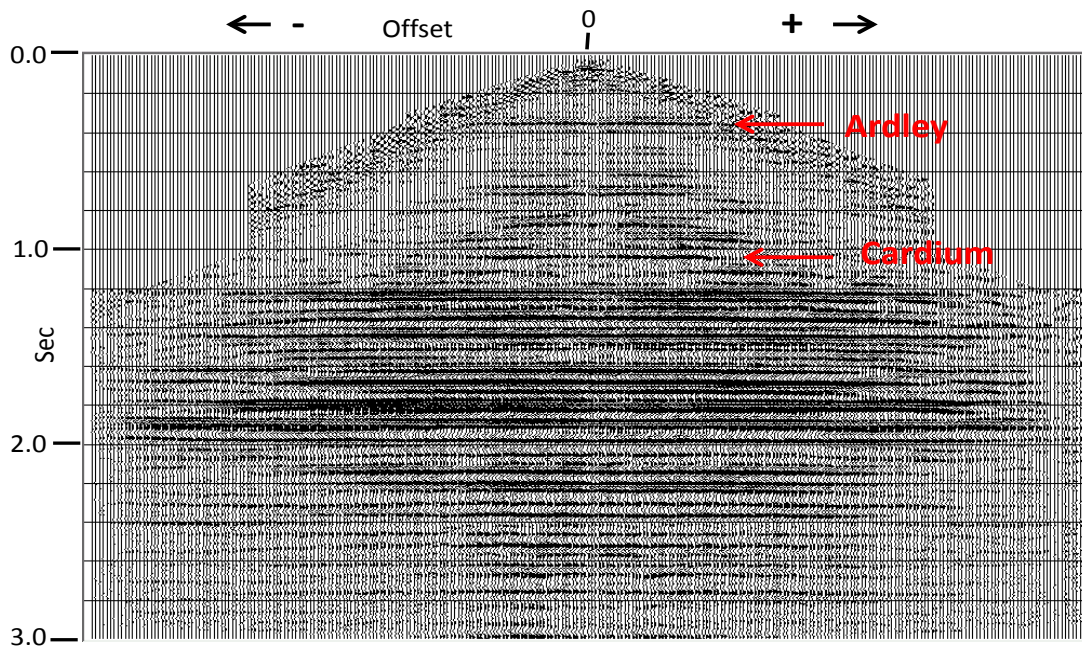


FIG. 18. Common-offset stack (CD₁₁ projection) for the 2D Violet Grove 'time-lapse' survey in 2007. Shading of deeper reflections by the strong Ardley reflection is visible.

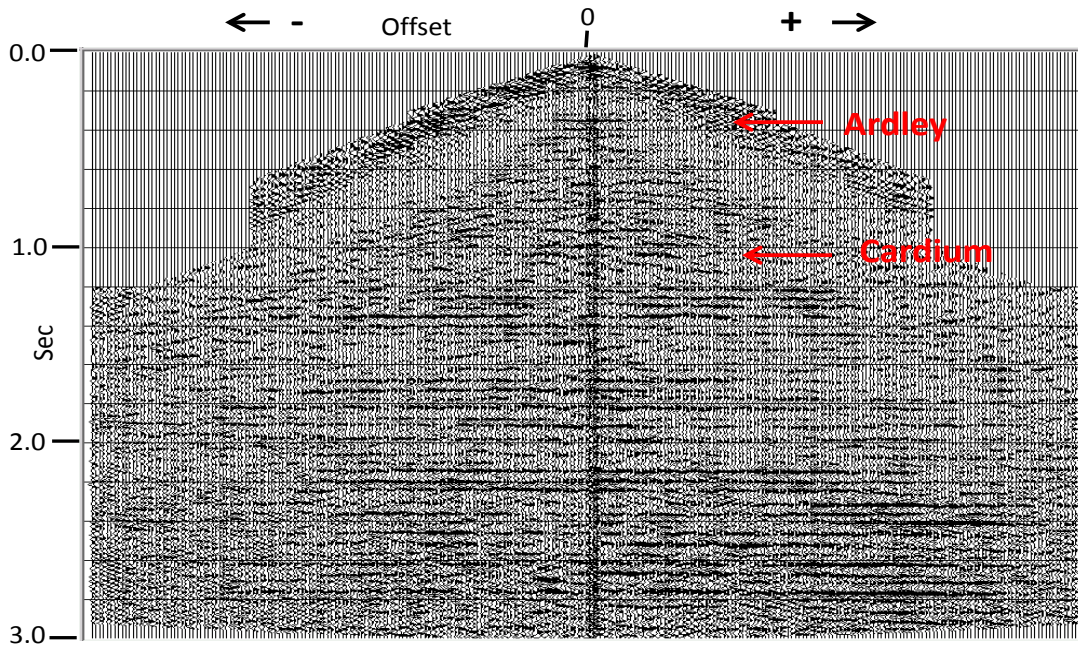


FIG. 19. Arithmetic difference between Figures 17 and 18. Systematic residuals for deeper reflections make any interpretation of an anomaly at the Cardium level questionable.

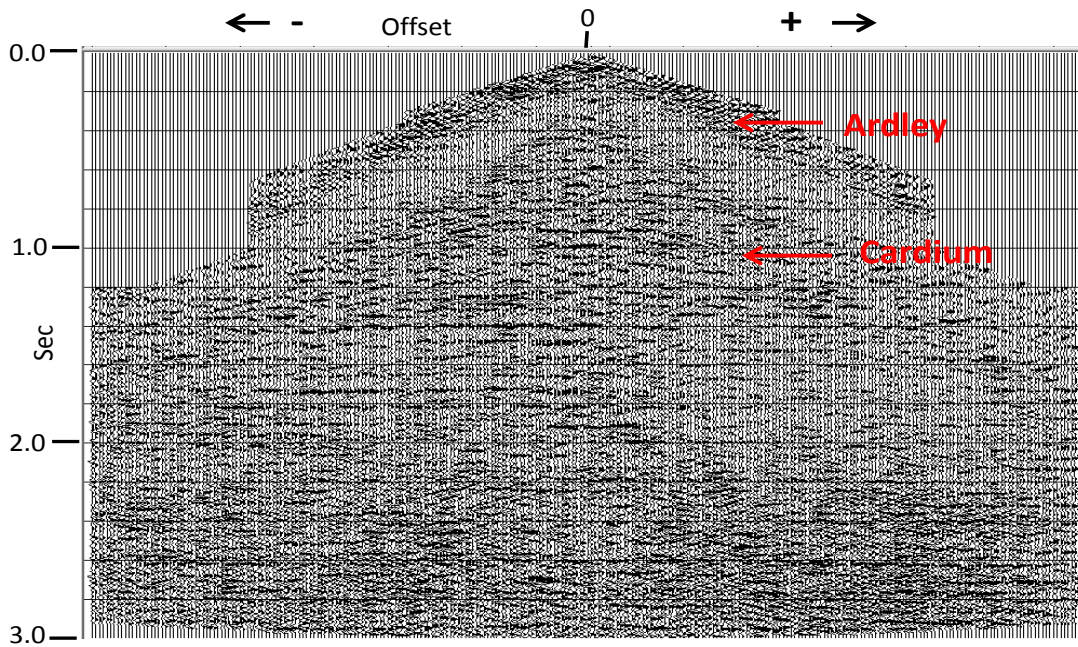


FIG. 20. Least-squares difference between Figures 17 and 18. Although systematic residuals are much reduced, anomaly at the Cardium level is still questionable.

Strange projections

Just to see what would happen, we transformed all the source gathers for both 2005 and 2007 surveys to the radial trace (RT) domain. The RT transform is a simple point-to-point mapping of amplitudes from the domain of travel time and lateral distance to a new domain of travel time and apparent velocity or raypath parameter (Claerbout, 1975). In the RT domain, an ensemble analogous to the common-offset gather is the common-raypath-parameter gather (also called the common-velocity gather, or the common-angle gather). Since the data on such gathers tend to share the same incidence angle at each reflector, they can be useful alternatives to common-offset gathers for AVO analysis. Thus, it makes sense to project a set of RT data along the common-raypath-parameter direction to obtain what we term ‘common-angle stacks’, as shown in Figures 21 and 22 for the 2005 and 2007 data sets, respectively. The Ardley and Cardium reflections are easily identified on both images, but the reflection amplitude ‘shading’ seen on the common-offset stacks seems much less prominent. The image difference is shown in Figure 23, where we can see slight apparent amplitude “blooms” at the Cardium level for small ray parameters on both sides of vertical. However, the large residual amplitude differences displayed over nearly all reflecting interfaces makes these anomalies questionable as time-lapse diagnostics. The least-squares difference image in Figure 24 shows no particular improvement.

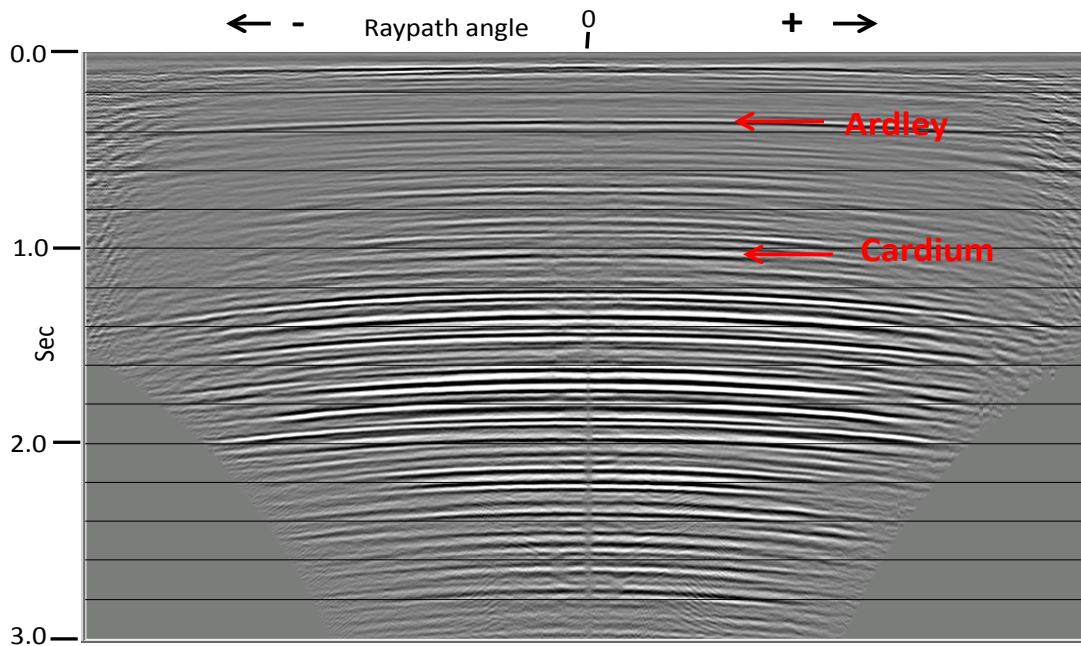


FIG. 21. Common-angle stack for the Violet Grove 2D ‘baseline’ survey in 2005.

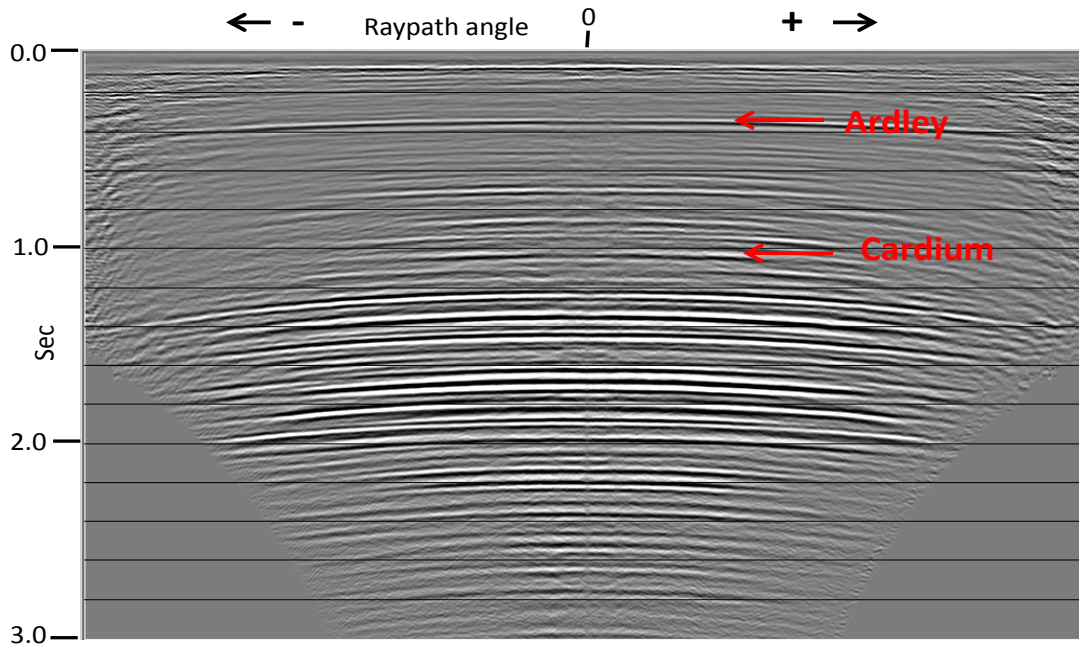


FIG. 22. Common-angle stack for the Violet Grove 2D 'time-lapse' survey in 2007.

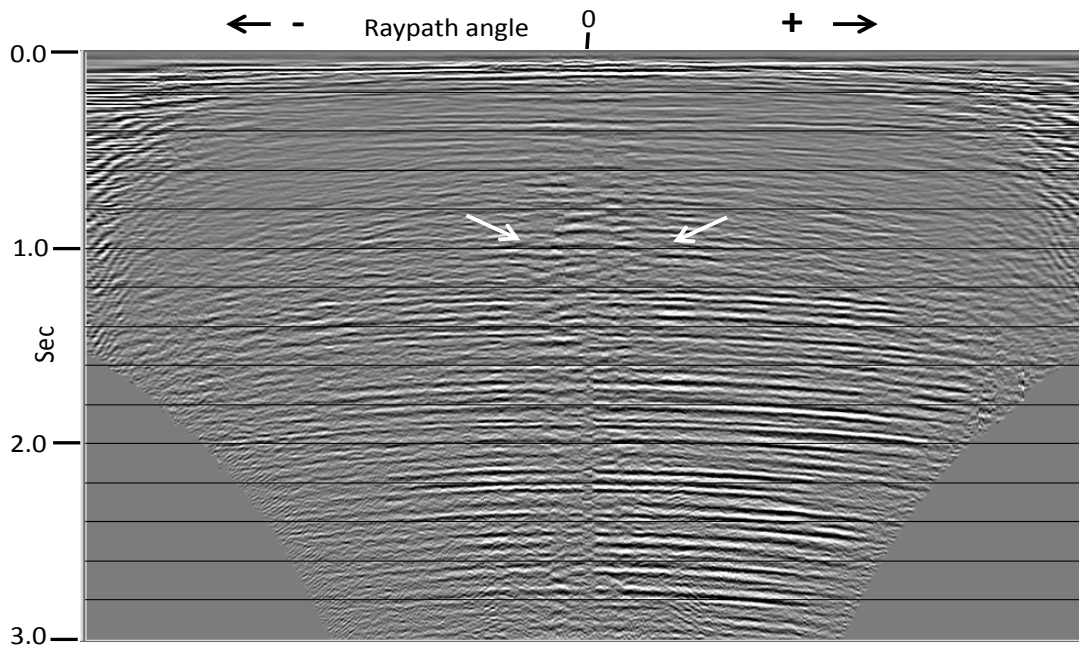


FIG. 23. Arithmetic difference between Figures 21 and 22. Although residuals from the deeper reflections are present, there are two distinct amplitude "blooms" at the Cardium that could indicate the anomaly.

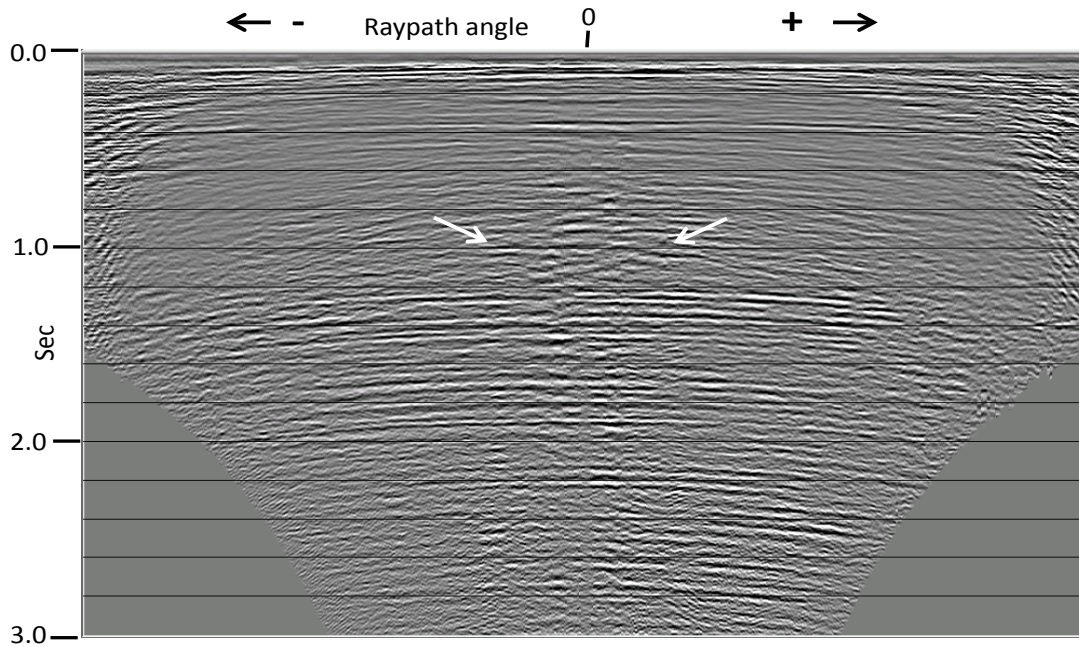


FIG. 24. Least-squares difference between Figures 21 and 22. Residuals are much reduced for the deeper reflections, and the Cardium anomalies are still visible.

As a matter of interest, the common-angle stack can be converted to a common-offset stack by applying the inverse RT transform. Figure 25 shows the inverse RT transform of the common-angle stack of the 2007 survey (Figure 21), and it can be compared directly to Figure 18, the common-offset stack for the same data. While the choice of offset bin size for the common-offset stack yields twice as many traces in Figure 18, it can be clearly seen that the amplitude variations on all reflectors is the same for both Figures 18 and 25. If we use the inverse RT transform to convert the common-angle difference image in Figure 23 to the common-offset stack difference, the result is Figure 26; and if we do the same conversion on Figure 24, the result is Figure 27. Disappointingly, neither of these images gives any more definitive identification of the time-lapse anomaly. Figure 28 is the colour version of Figure 27.

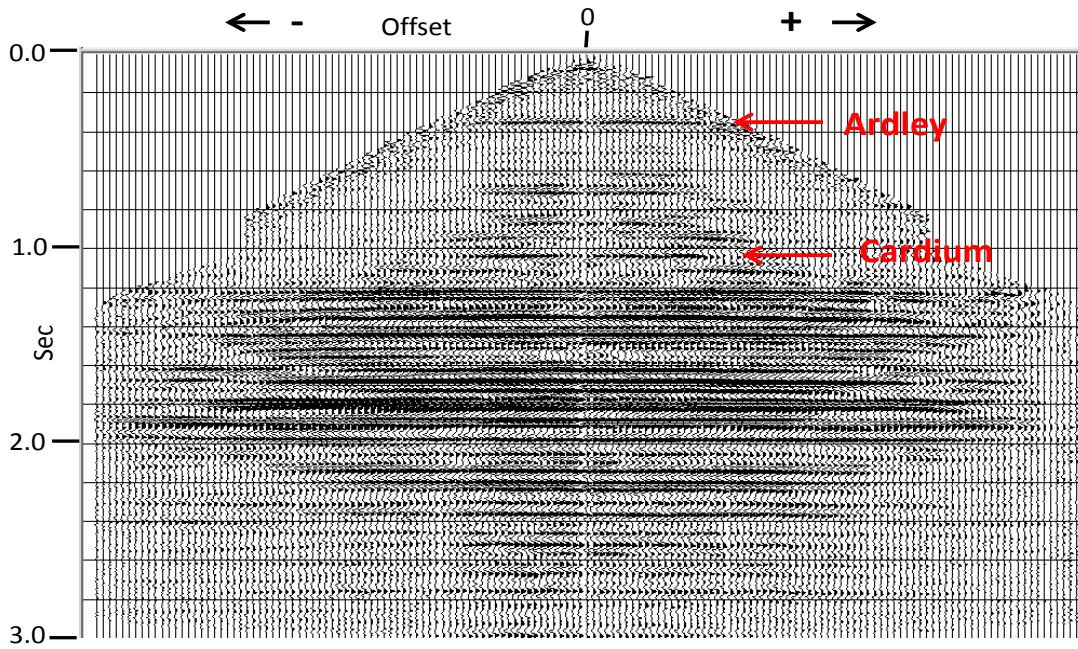


FIG. 25. Inverse RT transform of common-angle stack in Figure 21. Comparing this with Figure 17, the details are the same, regardless of the larger bin size in this figure.

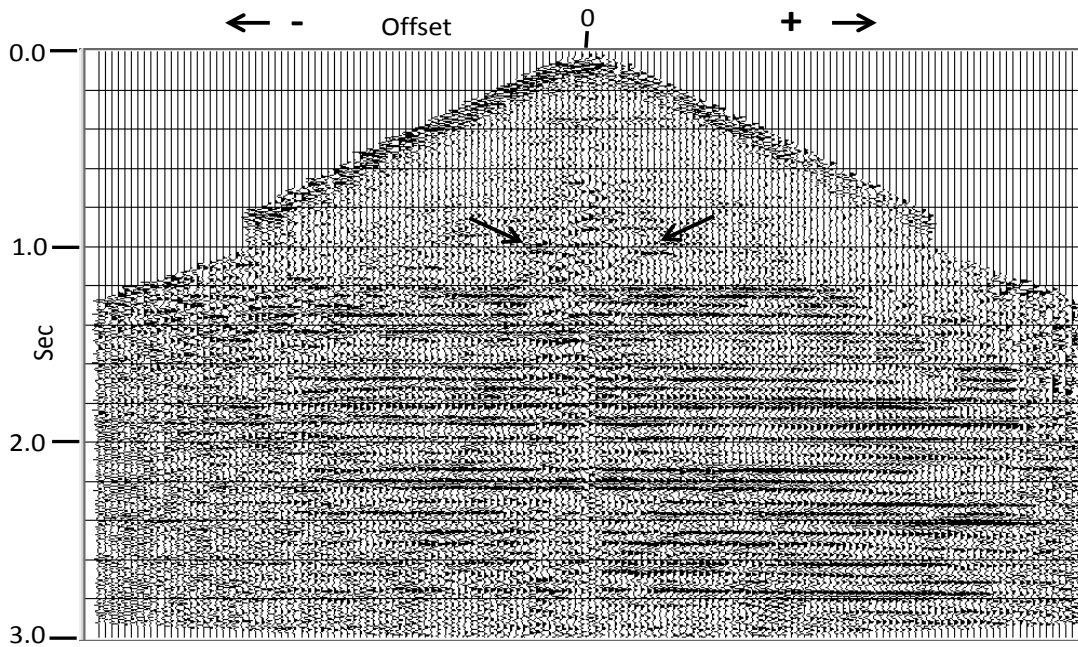


FIG. 26. Inverse RT transform of the common-angle stack difference in Figure 23. Cardium anomalies are visible, but amplitude of deep reflection residuals makes them questionable.

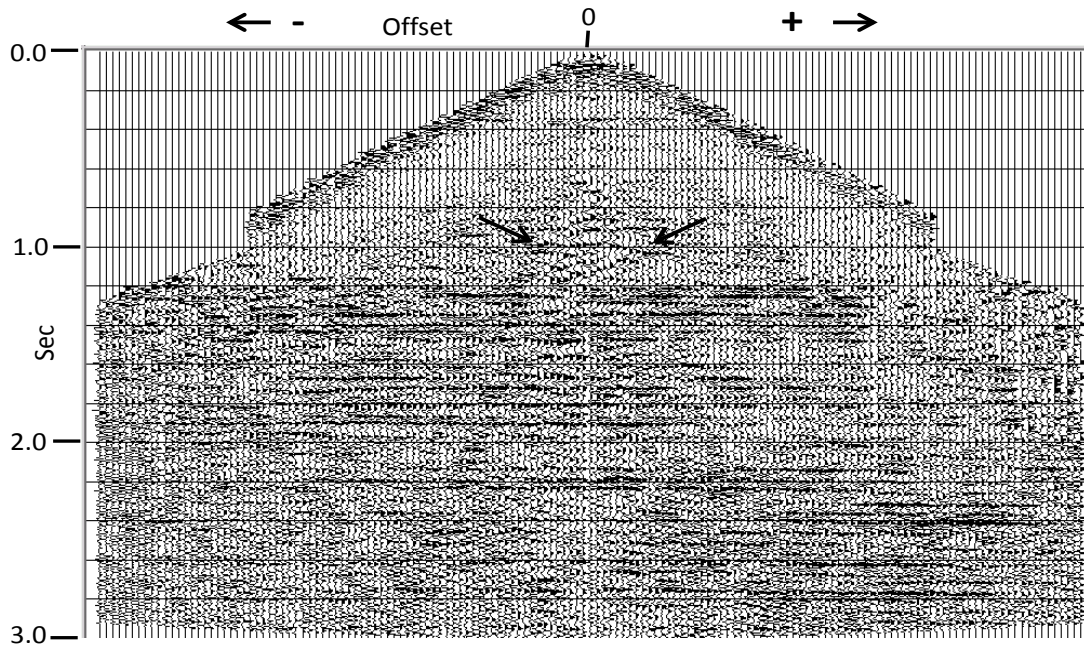


FIG. 27. Inverse RT transform of the least-squares common-angle stack difference in Figure 24. Deeper reflection residuals are reduced, Cardium anomalies remain unchanged.

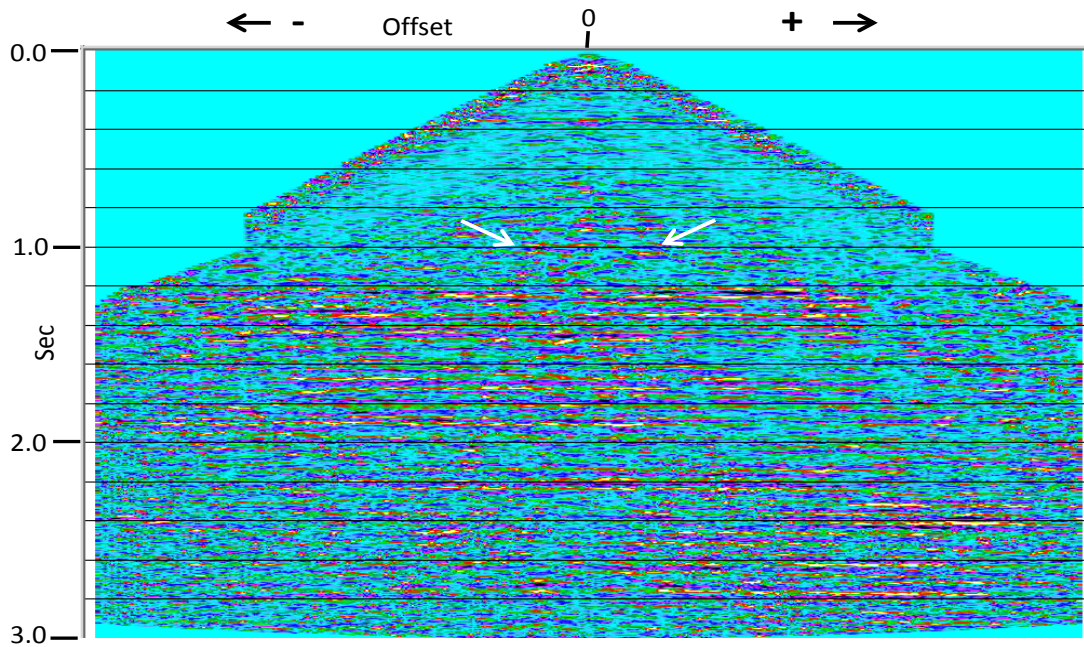


FIG. 28. Colour representation of Figure 27. In this format, the Cardium anomalies may be more visible relative to the reflection residuals beneath.

DISCUSSION

We have analyzed two 2D seismic data sets which were part of a time-lapse experiment performed in central Alberta over the time period 2005-2007. Our primary purpose was to demonstrate the use of various displays which are projections of the basic data sets. While we had hoped to provide unambiguous evidence of a time-lapse anomaly using one or more of our projection techniques, our analysis showed no particular improvement over more conventional techniques. It did, however, serve to illustrate some of the possibilities for enhancing various characteristics of seismic data using the general technique of projections.

In an earlier section, we also proposed a potential method for finding and applying non-stationary statics, using projections which we call focal-depth projections. This proposed method would, in fact, be a kind of hybrid projection tomography. The objective of this tomography would be to use the surface projections to correct for surface-consistent statics, then successively use deeper focal-depth projections to apply focal-depth-consistent statics, until the final projection would be the CMP projection of the reflections, with all statics anomalies removed.

ACKNOWLEDGEMENTS

The financial support of CREWES sponsors and NSERC is gratefully acknowledged. The author also acknowledges many helpful discussions with Mahdi Almutlaq during the analysis of the Violet Grove data.

REFERENCES

- Almutlaq, M.H., and Margrave, G.F., 2012, Violet Grove time-lapse data revisited: a surface-consistent matching filters application, CREWES Research Report **24**.
- Alshuhail, A., and Lawton, D.C., 2007, Time-lapse surface seismic monitoring of injected CO₂ at the Penn West CO₂-EOR site, Violet Grove, Alberta, CREWES Research Report **19**.
- Chen, F., and Lawton, D.C., 2005, Interpretation of baseline surface seismic data at the Violet Grove CO₂injection site, Alberta, CREWES Research Report **17**.
- Claerbout, J.F., 1975, Slant-stacks and radial traces: Stanford Expl. Project Report, **SEP-5**, 1-12.
- Coueslan, M.L., Lawton, D.C., and Jones, M., 2005, Baseline VSP processing for the Violet Grove CO₂ Injection Site, CREWES Research Report **17**.
- Lawton, D., Coueslan, M, Chen, F., Bland, H., Jones, M., Gallant, E., and Bertram, M., 2005, Overview of the Violet Grove CO₂seismic monitoring project, CREWES Research Report **17**.
- Lu, H-X., Hall, K., and Lawton, D.C., 2005, Violet Grove 2D and 3D data processing at CREWES, CREWES Research Report **17**.
- Radon, J., (1917), Über die Bestimmung von Funktionen durch ihre Integralwerte längs gewisser Mannigfaltigkeiten, Berichte über die Verhandlungen der Königlich-Sächsischen Akademie der Wissenschaften zu Leipzig, Mathematisch-Physische Klasse [Reports on the proceedings of the Royal Saxonian Academy of Sciences at Leipzig, mathematical and physical section] (Leipzig: Teubner) (**69**): 262–277; Translation: Radon, J.; Parks, P.C. (translator) (1986), On the determination of functions from their integral values along certain manifolds, IEEE Transactions on Medical Imaging **5** (4): 170–176, doi:10.1109/TMI.1986.4307775